Indirect noise prediction in compound, multi-stream nozzle flows

Khaled Younes, Jean-Pierre Hickey

Department of Mechanical and Mechatronics Engineering, University of Waterloo, Waterloo, Ontario, N2L 3G1, Canada

Abstract

An analytical framework to compute the acoustic response of one-dimensional planar waves in a compound-compressible nozzle is presented. Using the steady-state conservation equations, a set of algebraic relations governing compound flow is solved numerically. In each stream, the linearized Euler equations are recast using the invariant formulation and solved with a Magnus expansion following Duran & Moreau (*Journal of Fluid Mechanics* 723 (2013) 190–231). The modeled acoustic response is compared to the direct solution of the non-linear Euler equations with a maximum error of 5%. A parametric investigation of the acoustic response of a two-stream compound nozzle is presented. The effects of the bypass inflow Mach number and bypass ratio on the magnitude and phase of the transmitted and reflected acoustic waves are studied. It is shown that indirect noise generation is maximum in the peripheral bypass stream, not the core jet and that the initial Mach number of the bypass greatly impacts the phase shift of the resulting acoustic waves. The work provides an insight for acoustic response mitigation of high-speed confined jets.

Keywords: Aero-acoustics, Compound nozzle, Indirect noise, Combustion instabilities

1. Introduction

Over the past few decades, considerable efforts have been undertaken to characterize and reduce the noise emitted from ground and in-flight gas turbines. Of the various noise sources, it has been well-established that combustion noise is of great importance, see [1, 2] for recent reviews. Combustion noise in an aeroengine can be decomposed into direct and indirect noise. Direct noise arises due to the local density variation in the reactive flow region as a result of the unsteady heat release intrinsic to turbulent combustion. The generated acoustic perturbations from these volumetric expansions and contractions propagate through the turbine stages and exit the engine as direct noise. A summary of direct noise considerations can be found in [3, 4, 5, 6, 7, 8]. The unsteady, turbulent combustion also results in local vortical and entropic (hot and cold spots) inhomogeneities within the combustor. As the inhomogeneities are convected through the high-speed flow contractions–such as a nozzle or blade passage–their acceleration generates noise, which is referred to as *indirect noise*. Indirect noise can be a significant contributor to the total combustion noise [9, 10, 11, 12], is often associated with thermoacoustic instabilities [13, 14], and can lead to tonal noise generation in turbines [15, 16].

The original motivation to study indirect noise can be traced back to the necessity to compute transfer functions in rocket nozzles. The propagation of acoustic waves through a quasi-one-dimensional nozzle was first studied by Tsien [17] by assuming a linear velocity profile in the nozzle. The work was later extended by Marble & Candel [18] to include the propagation of entropy waves using a 'compact nozzle' approximation, which assumes a short nozzle relative to the wavelength of the perturbations. The compact nozzle assumption limits the analysis to low frequencies and cannot account for more complex nozzle geometries. To address these restrictions, Moase, Brear & Manzie [19] and Giauque, Huet & Clero [20] considered a piecewise-linear mean velocity profile while Stow, Dowling & Hynes [21] and Goh & Morgans [22] used an equivalent nozzle length correction. A more general approach to the problem was taken by Duran & Moreau [23], who proposed to use a Magnus expansion (Magnus [24]; Blanes *et al.* [25]) to solve the linearized Euler equations (*LEEs*) directly in the frequency domain. Their method allows the computation

Email address: j6hickey@uwaterloo.ca (Jean-Pierre Hickey)

of the linear transfer functions of an arbitrary, quasi-one-dimensional geometry and flow condition, at any frequency, for one-dimensional plane waves. An extension to analyze two-dimensional azimuthal waves was provided by Duran & Morgans [26]. The previously mentioned works all considered single-component, homogeneous gas mixtures. To account for compositional inhomogeneities in the flow, Magri *et al.* [27] first used the compact nozzle assumption in multi-component nozzle flows. Magri [28] later generalized the solution by performing an asymptotic expansion to the invariants of the compact nozzle solution.

The prediction of indirect noise has thus far only focused on single-stream nozzle flows. However, in most modern aeroengines, multiple gas streams–with different velocities, temperatures, and composition–are accelerated through geometric contractions. A similar multi-stream setup is encountered in jet- or rocket-engine test facilities (see, for example [29]). In these facilities, the high-speed engine exhaust entrains low-speed ambient air and both streams enter a flow contraction known as an augmenter tube. As the streams are differentially accelerated through the augmenter tube, it is expected that the convection of their flow inhomogeneities result in indirect noise. High-speed, multi-stream contractions are also found in supersonic ejector-mixer nozzles [30], which have been proposed as means to reduce jet noise in supersonic aircrafts [31]. With the exception of Yonamine *et al.* [32], who experimentally studied the propagation of weak pressure waves through a constant area duct, and Ferand *et al.* [33], who performed numerical simulations on a realistic dual-stream jet flow, the propagation of waves in multi-stream nozzles is not well understood despite its prevalence in industrial applications. The effect of a multi-stream, compressible nozzle flow–also classically referred to as *compound-compressible nozzle flow*–on the indirect noise generation and acoustic reflection has not yet been addressed and is the focus of the present work.

Compound-compressible nozzle flows were first studied by Pearson, Holliday & Smith [34] in the context of supersonic ejector nozzles. Hoge & Segars [35] were first to derive the general equation for choking of two or more co-flowing, unmixed streams, labeling it as the 'generalized choking' equation. Later, and in more detail, Bernstein, Heiser & Hevenor [36] investigated the problem and provided a one-dimensional theory based on fundamental flow relations, which was named 'compound-compressible flow' theory. They also showed that each stream in a compound nozzle is influenced by the presence of the other and introduced a compound-flow indicator (β) to illustrate the conditions for compound- subsonic, choked, and supersonic flow. An alternative approach using the generalized influence coefficients formulated by Shapiro [37] was used by Agnone [38] to arrive to the same choking condition as [36]. The confusion in the terminology associated with 'generalized choking' and 'compound choking' was addressed by Otis [39], who also presented a one-dimensional analysis of the mixing process between one supersonic stream and a subsonic stream in a two-stream compound-compressible nozzle. More recently, an experimental study was conducted by Kwon *et. al* [40] on dual subsonic stream flows with considerable mixing, providing visual insight on the phenomenon of compound choking.

This paper investigates analytically the propagation of one-dimensional planar acoustic and entropy waves in the linear regime through compound-compressible nozzle flows. The acoustic response is computed by solving the LEEs using the flow invariants and Magnus [24] expansion, as proposed by Duran and Moreau [23], combined with the compound-compressible nozzle relations derived by Bernstein, Heiser & Hevenor [36]. The computationally efficient approach resolves the equations in the frequency domain and permits a parametric investigation over the state space of arbitrarily complex compound nozzle flows. The paper is divided as follows: Section 2 presents the mathematical model used to solve for the propagation of waves through a single-stream nozzle and the extension to compound nozzles. Section 3 describes the validation steps taken by comparing the modeled response with analytical predictions and numerical simulations. Finally, results are presented in Section 4 and conclusions are drawn in Section 5.

2. Mathematical Model

2.1. Governing Equations

The quasi-one-dimensional Euler equations for a calorifically perfect gas can be written as

$$\frac{\partial}{\partial t}(\rho A) + \frac{\partial}{\partial x}(\rho u A) = 0, \tag{1}$$

$$\frac{\partial}{\partial t}(\rho u A) + \frac{\partial}{\partial x}\left(\left[p + \rho u^2\right] A\right) = p\frac{dA}{dx}, \tag{2}$$

$$\frac{\partial}{\partial t}\left(\left[\frac{p}{\gamma - 1} + \frac{1}{2}\rho u^2\right] A\right) + \frac{\partial}{\partial x}\left(\left[\frac{\gamma p}{\gamma - 1} + \frac{1}{2}\rho u^2\right] u A\right) = 0, \tag{3}$$

where u, p, ρ, and A are respectively the velocity, pressure, density, and cross-sectional area; the ratio of specific heat is denoted by $\gamma = c_p/c_v$. The variables of the Euler equations can be decomposed into a time-averaged mean quantity, $\bar{()}$, and a perturbation about the mean, $()'$, such that $() = \bar{()} + ()'$. Transport equations for the perturbations may be derived by neglecting the higher-order terms. The linearized Euler Equations read

$$\left[\frac{\partial}{\partial t} + \bar{u}\frac{\partial}{\partial x}\right]\left(\frac{p'}{\bar{\gamma}\bar{p}}\right) + \bar{u}\frac{\partial}{\partial x}\left(\frac{u'}{\bar{u}}\right) = 0, \tag{4}$$

$$\left[\frac{\partial}{\partial t} + \bar{u}\frac{\partial}{\partial x}\right]\left(\frac{u'}{\bar{u}}\right) + \frac{\bar{c}^2}{\bar{u}}\frac{\partial}{\partial x}\left(\frac{p'}{\bar{\gamma}\bar{p}}\right) + \left(2\frac{u'}{\bar{u}} - (\bar{\gamma} - 1)\frac{p'}{\bar{\gamma}\bar{p}} - \frac{s'}{\bar{c}_p}\right)\frac{\partial \bar{u}}{\partial x} = 0, \tag{5}$$

$$\left[\frac{\partial}{\partial t} + \bar{u}\frac{\partial}{\partial x}\right]\left(\frac{s'}{\bar{c}_p}\right) = 0, \tag{6}$$

where $\bar{c}$ is the mean flow speed of sound. For a calorifically perfect gas, the mean flow ratio of specific heats, $\bar{\gamma}$, and specific heat capacity, $\bar{c}_p$, are constants. Eqs. (4)–(6) can be written in dimensionless form using: $\chi = x/L$, where L is the nozzle length; $\tau = tf$, where f is a characteristic frequency of the perturbation; $\bar{M} = \bar{u}/\bar{c}$, where $\bar{M}$ is the mean flow Mach number; $\bar{\psi} = p'/(\gamma\bar{p})$, $\bar{v} = u'/\bar{u}$, and $\bar{\sigma} = s'/\bar{c}_p$, where $\bar{\psi}$, $\bar{v}$, $\bar{\sigma}$ represent the dimensionless pressure, velocity, and entropy fluctuations, respectively; and $\tilde{u} = \bar{u}/c_0$, where c_0 is a reference speed of sound. The Helmholtz number, $\omega = fL/c_0$, is introduced to relate the frequency of perturbations to the characteristic wavelength. The equations now read

$$\left[\omega\frac{\partial}{\partial \tau} + \tilde{u}\frac{\partial}{\partial \chi}\right](\bar{\psi}) + \tilde{u}\frac{\partial}{\partial \chi}(\bar{v}) = 0, \tag{7}$$

$$\left[\omega\frac{\partial}{\partial \tau} + \tilde{u}\frac{\partial}{\partial \chi}\right](\bar{v}) + \frac{\bar{c}^2}{\tilde{u}}\frac{\partial}{\partial \chi}(\bar{\psi}) + \left(2\bar{v} + (1 - \bar{\gamma})\bar{\psi} - \bar{\sigma}\right)\frac{\partial \tilde{u}}{\partial \chi} = 0, \tag{8}$$

$$\left[\omega\frac{\partial}{\partial \tau} + \tilde{u}\frac{\partial}{\partial \chi}\right](\bar{\sigma}) = 0. \tag{9}$$

Stow, Dowling & Hynes [21] and Goh & Morgans [22] performed an asymptotic expansion in ω for $\bar{u}$, $\bar{\rho}$, and $\bar{p}$ to obtain the non-compact response of a choked nozzle, correcting to first-order the compact solution of Marble & Candel [18]. A more general approach was taken by Duran & Moreau [23], who performed an asymptotic expansion in ω directly to the invariants of the compact solution derived by Marble & Candel [18]. In doing so, they corrected the compact solution with higher-order terms and arrived at a general solution that is applicable to arbitrary nozzle flows and geometries. For convenience, their solution procedure is briefly described next.

2.2. Generalized LEEs Solution

The invariants of the compact nozzle solution derived by Marble & Candel [18] are constant to first-order for any flow configuration. They are

$$I_A \equiv \frac{\dot{m}'}{\dot{m}} = \bar{\psi} + \bar{v} + \bar{\sigma}, \tag{10}$$

$$I_B \equiv \frac{T_t'}{T_t} = (\bar{\gamma} - 1)\frac{\bar{M}^2\bar{v} + \bar{\psi} + \dfrac{\bar{\sigma}}{\bar{\gamma} - 1}}{1 + \dfrac{\bar{\gamma} - 1}{2}\bar{M}^2}, \tag{11}$$

$$I_C \equiv \frac{s'}{\bar{c}_p} = \bar{\sigma}, \tag{12}$$

where $\dot{m}$, T_t, s represent mass flow rate, total temperature, and entropy, respectively. Using the definition of the mean flow Mach number, $\bar{M} = \bar{u}/\bar{c}$, reduced mean flow velocity, $\tilde{u} = \bar{u}/c_0$, substantial derivative, $D/D_\tau = \omega\dfrac{\partial}{\partial\tau} + \tilde{u}\dfrac{\partial}{\partial\chi}$, and by introducing the invariants of Eqs. (10)–(12) into Eqs. (7)–(9), the LEEs can be written as

$$\frac{D}{D_\tau}(I_A) = \frac{\tilde{u}}{(\bar{\gamma} - 1)\bar{M}^2}\left[\frac{\partial}{\partial\chi}(I_C) - \left(1 + \frac{\bar{\gamma} - 1}{2}\bar{M}^2\right)\frac{\partial}{\partial\chi}(I_B)\right], \tag{13}$$

$$\frac{D}{D_\tau}(I_B) = -\frac{(\bar{\gamma} - 1)\,\tilde{u}}{1 + \dfrac{\bar{\gamma} - 1}{2}\bar{M}^2}\left[\frac{\partial}{\partial\chi}(I_A) + \frac{\partial}{\partial\chi}(I_C)\right], \tag{14}$$

$$\frac{D}{D_\tau}(I_C) = 0. \tag{15}$$

Taking the time Fourier transform with $\mathrm{e}^{2\pi\mathrm{i}\omega\tau}$ of Eqs. (13)–(15) yields the following equation in matrix form

$$[\mathbf{E}(\chi)]\,\frac{\partial}{\partial\chi}\,[\mathbf{I}] = 2\pi\mathrm{i}\omega\mathbf{I}, \tag{16}$$

where $\mathbf{I}$ is the vector of invariants $[I_A, I_B, I_C]$ and $\mathbf{E}(\chi)$ is:

$$\mathbf{E}(\chi) = -\tilde{u}\begin{bmatrix} 1 & \dfrac{1 + \dfrac{\bar{\gamma} - 1}{2}\bar{M}^2}{(\bar{\gamma} - 1)\,\bar{M}^2} & \dfrac{1}{(\bar{\gamma} - 1)\,\bar{M}^2} \\ \dfrac{\bar{\gamma} - 1}{1 + \dfrac{\bar{\gamma} - 1}{2}\bar{M}^2} & 1 & \dfrac{\bar{\gamma} - 1}{1 + \dfrac{\bar{\gamma} - 1}{2}\bar{M}^2} \\ 0 & 0 & 1 \end{bmatrix}. \tag{17}$$

In Eq. (17), the mean flow Mach number, $\bar{M}$, and the dimensionless velocity, $\tilde{u}$, are functions of the non-dimensional space variable, χ. The matrix system presented in Eq. (16) can be inverted when the Mach number $\bar{M} \neq 1$. The resulting matrix equation can then be solved by performing an asymptotic expansion in terms of the invariants and using the Magnus [24] expansion, as proposed by Duran & Moreau [23]. The boundary conditions for the incoming and outgoing propagating waves are shown in Fig. 1: α^+ and α^- correspond to the downstream- and upstream-propagating acoustic waves, respectively, and β is the entropy wave; the superscripts $()^i, ()^t, ()^e$ represent the inlet, throat, and exit planes of the nozzle, respectively. A detailed description of the application of these conditions is given in [23] and is not repeated here for brevity.

When the nozzle is choked, $\bar{M} = 1$ at the throat and Eq. (16) cannot be inverted because of a singularity. To solve the choked case, the nozzle is divided into two sections: a convergent and a divergent section. Both sections are separated by an infinitesimally small distance, ϵ. The perturbations in the subsonic section of the nozzle are calculated

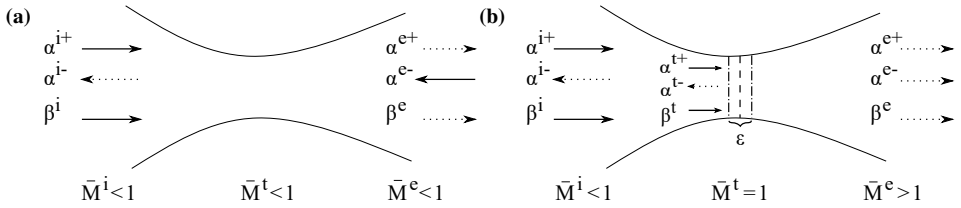

Fig. 1. Representation of the downstream-propagating acoustic wave, α^+, upstream-propagating acoustic wave, α^-, and entropy wave, β, in (a) subsonic nozzle and (b) supersonic nozzle, where $()^i, ()^t, ()^e$ represent the inlet, throat, and exit of the nozzle, respectively.

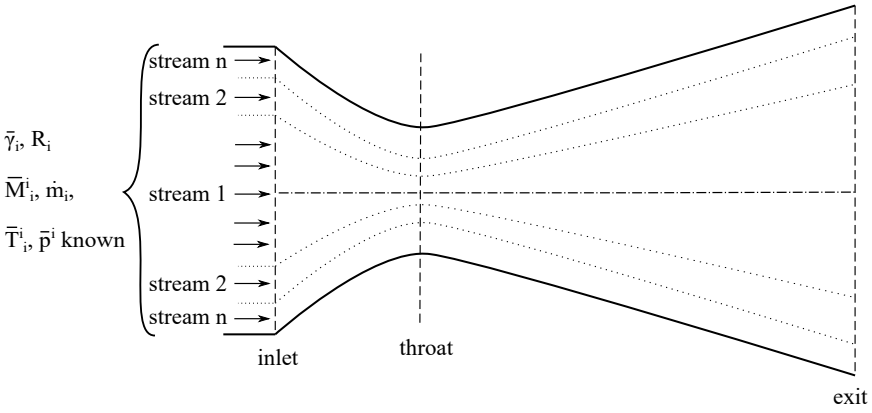

Fig. 2. Diagram of an axially symmetric n-stream compound nozzle, where the superscript $()^i$ refers to the axial position (e.g. inlet, exit) while the subscript $()_i$ refers to the i-th stream.

at $\bar{M} = 1 - \epsilon$ and applied as input to the supersonic flow at $\bar{M} = 1 + \epsilon$, where $\epsilon \ll 1$. At the throat, Marble & Candel [18] and Stow, Dowling & Hynes [21] showed that the compact assumption holds. Thus, the boundary condition $M'/M = 0$ could be applied and if the limit $\epsilon \to 0$ is taken, the reflection coefficients and input perturbations to the divergent section of the nozzle can be found

$$\alpha^{t-} = R_\alpha \alpha^{t+} + R_\beta \beta^t, \tag{18}$$

$$R_\alpha = \frac{3 - \bar{\gamma}}{1 + \bar{\gamma}}, \tag{19}$$

$$R_\beta = \frac{-2}{1 + \bar{\gamma}}. \tag{20}$$

In terms of dimensionless fluctuations, the downstream-propagating acoustic wave can be written as: $\alpha^+ = \bar{\psi} + \bar{M}\bar{v}$, the upstream-propagating acoustic wave as: $\alpha^- = \bar{\psi} - \bar{M}\bar{v}$, and the entropy wave as: $\beta = \bar{\sigma}$.

2.3. Extension to Compound-Compressible Nozzle Flow

To account for multiple streams in the nozzle exhaust, we follow the formulation proposed by Bernstein, Heiser & Hevenor [36]. This formulation is chosen because: (1) it remains tractable for the intended computations, (2) it is the standard model discussed in recent turbomachinery textbooks, see for example [41, chap. 10], and (3) predictions compare well with results from three-dimensional numerical simulations and experimental measurements [36]. First, we apply the geometric constraint governing the cross-sectional area of each stream. By assuming that mixing between the streams is negligible, the area occupied by each stream is

$$\sum_{i=1}^{n} A_i(x) = A_t(x); \qquad \sum_{i=1}^{n} \frac{\mathrm{d}}{\mathrm{d}x} A_i(x) = \frac{\mathrm{d}}{\mathrm{d}x} A_t(x), \tag{21}$$

where i represents the *i-th* stream, n the total number of streams, and $A_t(x)$ the total cross-sectional area of the nozzle. We then introduce the equation of state and isentropic nozzle flow relations as follows

$$\bar{p}_i = \bar{\rho}_i R_i \bar{T}_i, \tag{22}$$

$$\frac{p_{o,i}}{\bar{p}_i} = \left(1 + \frac{\bar{\gamma} - 1}{2}\bar{M}_i^2\right)^{\frac{\bar{\gamma}}{\bar{\gamma} - 1}} = \left(\frac{T_{o,i}}{\bar{T}_i}\right)^{\frac{\bar{\gamma} - 1}{\bar{\gamma}}}, \tag{23}$$

where R_i is the gas constant of the *i-th* stream and $p_{o,i}, T_{o,i}$ represent the stagnation pressure and temperature conditions of the *i-th* stream, respectively. Note that for steady, adiabatic, and isentropic flows, R_i, $p_{o,i}$, and $T_{o,i}$ are constant in each stream. By assuming that the area change in the nozzle, $\mathrm{d}A_i/\mathrm{d}x$, is small, the mean flow pressure, $\bar{p}_i$, becomes only a function of the axial position along the nozzle. Using Eqs. (22)–(23), the mass flow rate of the *i-th* stream can then be written as

$$\dot{m}_i = \frac{A_i p_{oi}}{\sqrt{T_{oi}}}\left(\frac{\bar{p}}{p_{oi}}\right)^{\frac{1}{\bar{\gamma}_i}} \sqrt{\frac{2}{R_i}\left(\frac{\bar{\gamma}_i}{\bar{\gamma}_i - 1}\right)\left[1 - \left(\frac{\bar{p}}{p_{oi}}\right)^{\frac{\bar{\gamma}_i - 1}{\bar{\gamma}_i}}\right]}, \tag{24}$$

where the mean flow pressure of each stream, $\bar{p}_i$, has been replaced by the global mean flow pressure in the nozzle, $\bar{p}$, under the aforementioned assumption. By combining Eq. (24) with the geometric constraint given in Eq. (21), the system of algebraic equations governing compound nozzles could be solved to yield the pressure variation along the nozzle length for a given set of initial conditions. The Mach number distribution of each stream can then be obtained by applying Eq. (23). To get the frequency response of the compound-compressible nozzle, we solve the LEEs in invariant form, Eqs. (13)–(15), for each stream–by inverting Eq. (17) and using the Magnus expansion [24, 25]–and apply the appropriate boundary conditions, as given by Fig. 1.

An n-stream compound-compressible nozzle can be represented as shown in Fig. 2. The problem is fully defined for a given nozzle geometry, $A_t(\chi)$, gas composition, $\bar{\gamma}_i, R_i$, initial mean flow Mach number, $\bar{M}_i^i$, mass flow rate, $\dot{m}_i$, and temperature, $\bar{T}_i^i$, of each stream, and dynamic pressure at the inlet, $\bar{p}^i$. In the special case of a two-stream compound nozzle ($n = 2$), it is conventional in the gas turbine community to define the bypass ratio as BPR $= \dot{m}_2/\dot{m}_1$, where $\dot{m}_1$ is the mass flow rate of the main, high-speed flow (often referred to as *jet*) and $\dot{m}_2$ is the mass flow rate of the secondary, low-speed, peripheral flow (often referred to as *bypass*). See, for example, terminology used in [42]. This convention is followed hereafter.

3. Validation of low-order modeling

The developed multi-stream framework hinges on three fundamental assumptions. First, the mean pressure is assumed constant in the radial direction at each axial location: $\bar{p}_i(x) = \bar{p}(x)$; this assumption is implicit in the compound relations and it holds for attached flow with modest accelerations through the nozzle. Second, the shear layer between the streams acts as a waveguide to the planar perturbations. In other words, the acoustic perturbations in each stream can be considered to be independent. In the limit of high wavenumbers and perturbation Mach numbers, similar to the ones considered in this study, Hau [43] showed that acoustic waves cannot penetrate through the shear layer and are redirected back onto the originating flow. An analogous effect is also observed in a transitional, compressible planar wake, where the shear layers on either side of the wake act as waveguides to the propagating acoustic instabilities [44]. These findings support our waveguide assumption. Third, the streams do not mix and are perfectly inviscid. As the framework employs an Euler solver as a proxy for very high-Reynolds number flows, the relative importance of mixing between the streams is negligible. Due to the lack of publicly available experimental data on the acoustic responses of compound nozzle flows, the mathematical model is validated analytically and numerically.

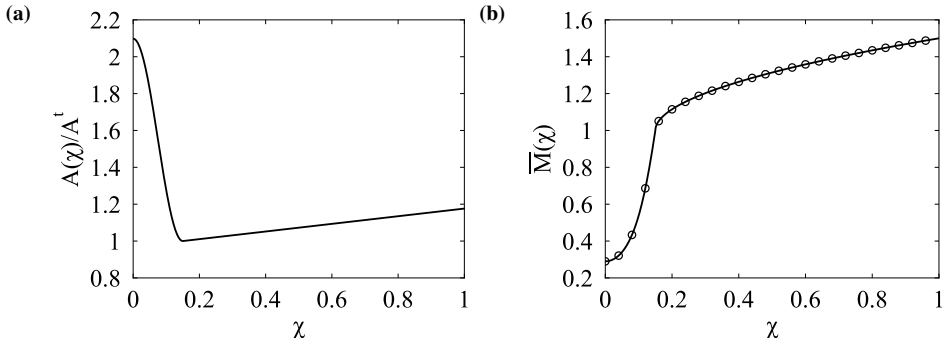

Fig. 3. (a) Nozzle geometry of Duran & Moreau [23] and (b) mean flow Mach number distribution for the choked condition, where $\bar{M}^i_{\text{jet}} = \bar{M}^i_{\text{bypass}} = 0.29$. (–): compound solver; (○): Duran & Moreau [23]. Results from [23] were taken from the online version of their paper.

3.1. Comparison with the analytical solution of Duran & Moreau

Duran & Moreau [23] derived the general analytical solution for single-stream nozzle flows, as presented in Section 2.2. Their major assumptions were the consideration of only quasi-one-dimensional planar waves and neglecting of viscous terms. They validated their model by comparing the results obtained with experimental data gathered by Bell *et. al* [45]. Since a single-stream nozzle is a special case of a multi-stream nozzle (where $n = 1$), the mathematical model derived in Section 2 could be validated against their results. In this subsection, the nozzle profile chosen is similar to that proposed in [23] for real nozzles (Fig. 3a).

A single-stream nozzle flow is fully defined by the location of the throat, $\chi^t = 0.15$, inlet mean flow Mach number, $\bar{M}^i = 0.29$, and exit mean flow Mach number, $\bar{M}^e = 1.5$. An equivalent two-stream compound nozzle flow is fully described by six parameters at the inlet: mean flow Mach number of each stream, $\bar{M}^i_{\text{jet}} = \bar{M}^i_{\text{bypass}} = 0.29$, bypass ratio, BPR = 1.0, mean flow temperature of each stream, $\bar{T}^i_{\text{jet}} = \bar{T}^i_{\text{bypass}} = 373$ K, and dynamic pressure, $\bar{p}^i = 1$ atm. As each stream has identical flow characteristics, we show that our model reverts back to a single-stream solution in the limit case of multiple identical streams. The mean flow Mach number distribution is shown in Fig. 3b for both nozzles. The response due to a downstream-propagating acoustic wave at the inlet is plotted in Fig. 4 using both models. Since the Mach number reaches sonic conditions at the throat, two acoustic waves are produced: an upstream-propagating wave at the inlet, α^{i-}, and a downstream-propagating wave at the exit, α^{e+}. As can be seen, the magnitude and phase of the waves (in both streams) are in perfect agreement with the single-stream nozzle solution of Duran & Moreau [23].

3.2. Comparison with numerical simulations

The assumptions made in the derivation of the compound solver are assessed by a direct solution of the fully non-linear Euler equations [46], on a well-defined geometry without flow separation. Here, the NASA Converging-Diverging Verification (*CDV*) nozzle is used, see details in [47, chap. 5]. The nozzle geometry is plotted in Fig. 5a. A dual-stream compound flow is set up with a jet stream occupying an inner radius of 0.5R ($A^i_{\text{jet}}/A^i_t = 0.25$); the remaining area is allocated to the bypass stream: $A^i_{\text{bypass}}/A^i_t = 0.75$. For the nonlinear, laminar, dual-stream simulations, we use OpenFOAM v17.12 with a fully structured mesh on an axisymmetric domain. The mesh, shown in Fig. 6, is grid-independent with a total of 6500 points; 1500 grid points are used in the axial direction. The discretization is handled using the second-order accurate central differencing scheme. For the time-averaged base flow, time stepping is achieved by the first-order, implicit, forward Euler method using a Courant-Friedrichs-Lewy (*CFL*) number of 0.55. Fig. 5b shows the Mach number distribution obtained from the low-order model and numerical solver for an initial mean flow Mach number of $\bar{M}^i_{\text{jet}} = 0.27$ for the jet and $\bar{M}^i_{\text{bypass}} = 0.17$ for the bypass, BPR = 2.0, inlet temperatures, $\bar{T}^i_{\text{jet}} = \bar{T}^i_{\text{bypass}} = 298$ K, and exit pressure, $\bar{p}^e = 1$ atm. Excellent agreement is obtained for the compound flow relations described in the previous section. The acoustic response obtained from the low-order model is then compared against the direct solution of the non-linear Euler equations (Fig. 7). The flow in each stream is independently perturbed by a small amplitude sinusoidal acoustic oscillation at the inlet once the base flow transient simulation has stabilized. To avoid spurious acoustic reflections, a non-reflective, *waveTransmissive* [48] boundary condition is implemented at

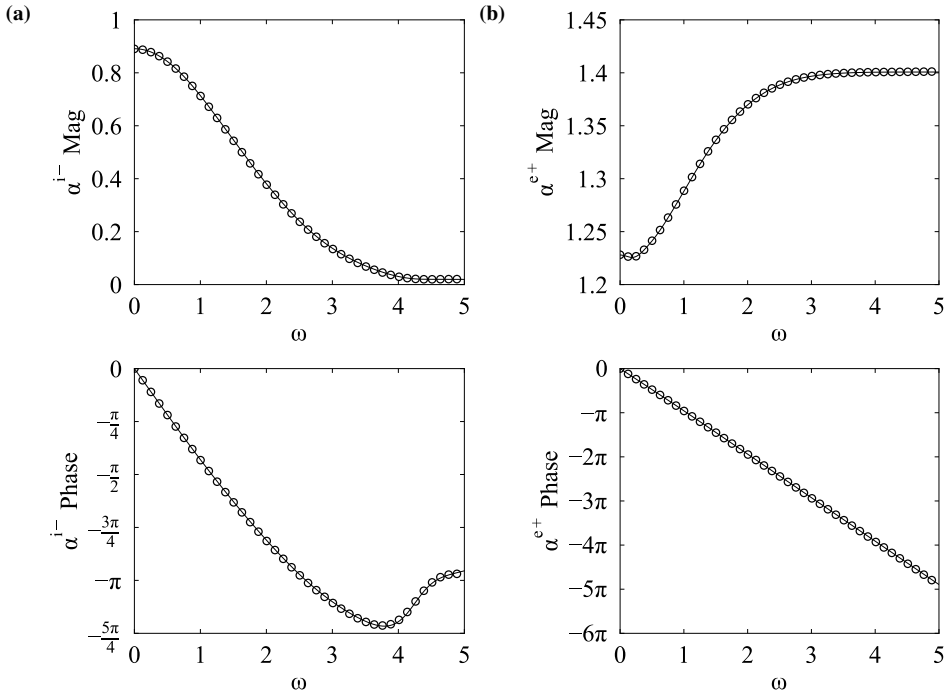

Fig. 4. Magnitude and phase of the (a) reflected upstream-propagating acoustic wave at the inlet α^{i-} and (b) downstream-propagating acoustic wave at the exit α^{e+} caused by a unitary downstream-propagating acoustic wave at the inlet $\alpha^{i+} = 1.0$. (–): compound solver; (○): Duran & Moreau [23]. Results from [23] were taken from the online version of their paper.

the inlet and outlet. The waveTransmissive boundary condition in OpenFOAM v17.12 is a simplification of the non-reflective Navier-Stokes Characteristic Boundary Condition (*NSCBC*) of Poinsot & Lele [49]. Again, the governing equations are solved in conservative form with a finite-volume scheme using central differencing without artificial viscosity. However, time stepping is now carried out using the second-order Crank-Nicolson method with an acoustic CFL number of 0.04. For each frequency, the simulation is run long enough to ensure that the response is periodic with at least 5 flow through times. The centreline temporal pressure and velocity fluctuations for each stream are extracted and a Fast-Fourier Transform (*FFT*) [50] is applied to yield the frequency response of the compound nozzle. Given the limited scale separation of the problem (no turbulence) and ability to adapt the mesh resolution to the perturbation waves, a relatively low-order finite-volume scheme is deemed appropriate. Generally, low-order schemes present unfavorable dispersive and dissipative characteristics for acoustic propagation, but since we use over 650 grid points per wavelength in the streamwise direction, the resulting numerical error at the frequencies under consideration is small. It was shown in Appendix A by a modified wave number analysis that the dispersion and dissipative errors do not exceed 2%. Despite the non-linearity of the two-dimensional simulations, the responses are in general in good agreement over most wavelengths investigated, with a maximum error of 5%. Such discrepancy in the numerical results is not uncommon and a similar magnitude error was observed in the numerical results presented in [20]. These validation results give us confidence in the assumptions made to derive our low-order acoustic model.

4. Results

In this section, the mathematical model presented in Section 2 is used to quantify the relative contribution of a secondary stream on the indirect noise generated in two-stream compound-compressible nozzles. Again, we note that this model is only valid for inviscid isentropic flows without appreciable mixing, flow separation, and radial pressure differences. First, the compound flow is perturbed by a unitary entropic perturbation convecting from the inlet, and the transmitted and reflected acoustic waves are computed for each stream. Here, the transmitted waves are a measure of indirect noise, whereas the reflected waves are important in the study of low-frequency thermoacoustic instabilities

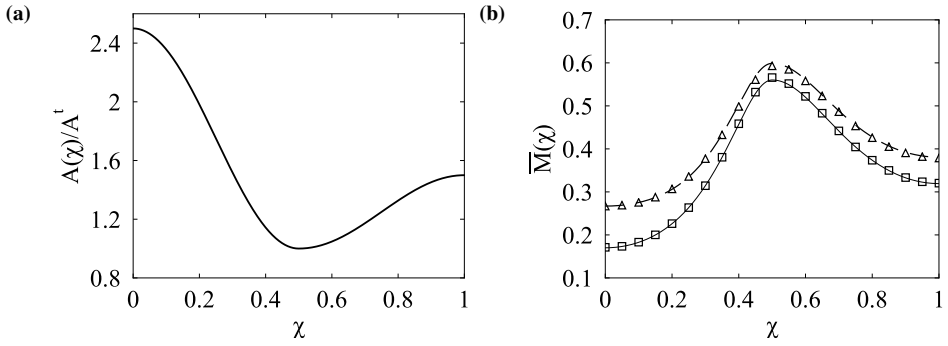

Fig. 5. (a) Nozzle geometry and (b) mean flow Mach number distribution through the CDV nozzle for the compound case. (— —): analytical jet solution, (△): numerical jet solution; (——): analytical bypass solution, (□): numerical bypass solution.

[13, 14, 51]. Then, the acoustic transfer functions are obtained to complement the analysis. We distinguish between *indirect noise*, which is the acoustic response due to an entropy perturbation, and an *acoustic transfer function*, which is the acoustic response due to an acoustic perturbation. In all cases studied, the Magnus expansion is performed up to 5^{th}-order, in which the infinite series was shown to converge in [23], and up to $\omega \to 2$. This range of frequency is selected such that nonlinear perturbations at low frequencies can be neglected. A fully converged, grid-independent solution using 20,000 nozzle subdivisions with equal spacing is also verified.

For simplicity, the geometry considered here is that studied by Duran & Moreau [23]. The nozzle is characterized by a narrow converging section and a long diverging section to prevent flow separation (Fig. 3a). Two distinct streams of the same fluid ($\bar{\gamma}^i_{\text{jet}} = \bar{\gamma}^i_{\text{bypass}} = \bar{\gamma}_{\text{air}} = 1.4$) at the same temperature are considered. The noise generated from compositional inhomogeneities in the flow, which could arise due to incomplete mixing in the combustion chamber, air dilution, or variations in the mixture gas composition (different $\bar{\gamma}^i$) was studied in [27, 28]. The temperature dependence on the acoustic response will be considered in future work. The initial conditions at the inlet are taken to be $\bar{p}^i = 216$ kPa and $\bar{T}^i_{\text{jet}} = \bar{T}^i_{\text{bypass}} = 986$ K, corresponding to typical combustion chamber outlet conditions of an idle aeroengine. The nozzle is choked under the condition of $\bar{M}^i_{\text{jet}} = \bar{M}^i_{\text{bypass}} = 0.29$.

To isolate the effects of the bypass stream on the acoustic response of the compound nozzle, a parametric study is conducted. The inflow Mach number of the bypass stream is varied in the low subsonic regime between [0.05–0.15] while fixing the jet inflow Mach number at 0.29 and bypass ratio at 1.0. Additionally, since in a compound nozzle the area occupied by each stream at the inlet affects the evolution of the mean flow Mach number, the bypass ratio is also varied between [0.5–1.5] at constant inflow Mach numbers of 0.29 for the jet and 0.2 for the bypass. Table 1 provides a summary of the cases studied. The resulting Mach number distribution through the nozzle is shown in Fig. 8. A general trend in the plots is noted–namely, higher bypass Mach numbers or lower bypass ratios (smaller areas occupied by the bypass) at the inlet result in stronger accelerations and decelerations of the flow upstream and downstream of the throat, respectively. This is due to the fact that, under the constant radial pressure assumption (recall that the temperature of both streams is identical for all cases), the mean flow Mach number distribution of each stream is directly proportional to the mass flow rate, which increases with the bypass inflow Mach number, and inversely proportional to the area occupied, which decreases as the bypass ratio decreases (Table 1). The effect of this phenomenon on the acoustic response of the compound nozzle is explored next.

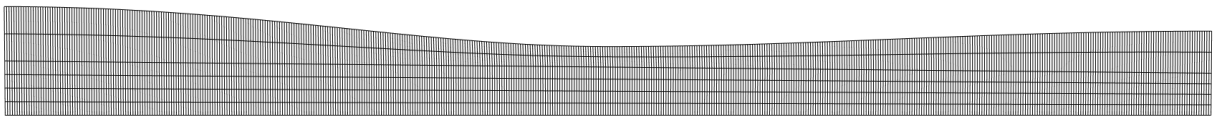

Fig. 6. Computational mesh for the CDV nozzle.

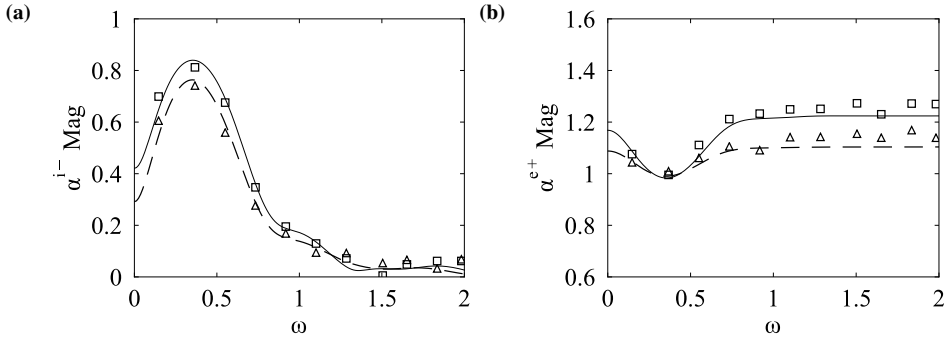

Fig. 7. Comparison of numerical and analytical results generated by a unitary downstream-propagating acoustic wave at the inlet, $\alpha^{i+} = 1.0$, for the CDV nozzle: (a) α^{i-} (b) α^{e+}. (——): analytical jet solution, (△): numerical jet solution; (——): analytical bypass solution, (□): numerical bypass solution.

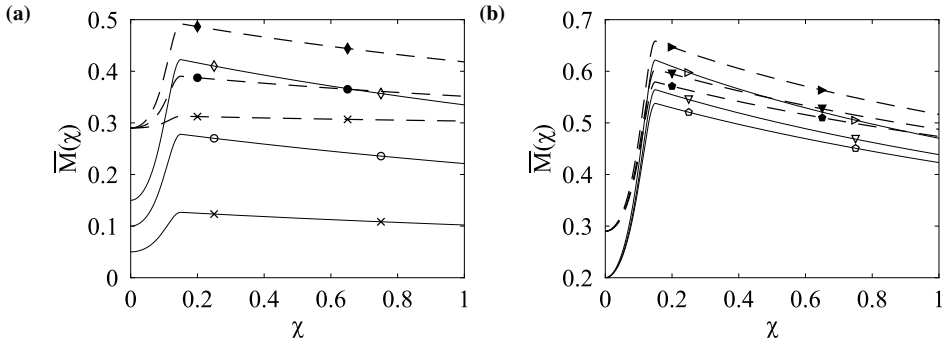

Fig. 8. Mean flow Mach number distribution for the conducted parametric study obtained by varying the (a) initial bypass Mach number through (×): $\bar{M}^i_{\text{bypass}} = 0.05$, (○, ●): $\bar{M}^i_{\text{bypass}} = 0.1$, and (◇, ◆): $\bar{M}^i_{\text{bypass}} = 0.15$ at a constant $\bar{M}^i_{\text{jet}} = 0.29$ and BPR = 1.0; and (b) bypass ratio through (▷, ▶): BPR = 0.5, (▽, ▼): BPR = 1.0, and (⬠, ⬟): BPR = 1.5 at a constant $\bar{M}^i_{\text{jet}} = 0.29$ and $\bar{M}^i_{\text{bypass}} = 0.2$. Dashed lines (——) refer to the jet stream; solid lines (——) refer to the bypass.

4.1. Response due to an entropy excitation

Figs. 9 and 10 show the acoustic response caused by an entropy excitation at the inlet for bypass Mach numbers in the range of $\bar{M}^i_{\text{bypass}} = [0.05–0.15]$ and bypass ratios, BPR, between [0.5–1.5]. It can be seen that indirect noise generation is greater in the secondary, low-speed bypass stream up to a certain threshold frequency, ω_{th}. The threshold frequency appears to be dictated by the Mach number distribution of each stream through the nozzle, which is in turn sensitive to changes in inflow conditions and nozzle geometry. Since the nozzle studied in this section has a small expansion ratio to prevent flow separation, gradual flow decelerations are observed in the diverging section. However, since the nozzle remains subsonic, the flow is sensitive to gradients at both the upstream and downstream locations. Thus, it is expected that ω_{th} will strongly depend on the Mach number evolution in the narrow converging section. Indeed, the threshold frequency shifts to the right, towards higher frequencies, as the difference in upstream mean flow gradients between the bypass and jet stream decreases. Physically, ω_{th} indicates the degree of asymmetry of the streams in the compound nozzle; $\omega_{\text{th}} \to \infty$ when the compound nozzle is perfectly symmetric, i.e., when the Mach number profile of both streams is identical. The increased noise generation from the bypass could then be attributed to the stronger acceleration of the flow upstream of the throat. Since entropy noise is a dipole source [18], its strength increases with larger mean flow gradients. In the case of a compound nozzle, larger mean flow gradients are present in the low-speed, peripheral bypass flow and thus, it generates more noise. This also explains why the responses amplify as the inflow Mach number of the bypass increases or bypass ratio decreases.

The reflected acoustic waves (Figs. 9a and 10a) show a different behavior. The responses from both streams decrease monotonically with increasing frequency, indicating that the acoustic energy loss through the boundary increases at higher frequencies. It is the propagation of these waves through the high-pressure turbine and back to

Table 1
Summary of cases studied by varying the inflow bypass Mach number and bypass ratio.

Case	$\bar{M}^i_{\text{jet}}$	$\bar{M}^i_{\text{bypass}}$	BPR	A^i_{jet}/A_t	A^i_{bypass}/A_t
1	0.29	0.05	1.0	0.15	0.85
2	0.29	0.10	1.0	0.25	0.75
3	0.29	0.15	1.0	0.35	0.65
4	0.29	0.20	0.5	0.55	0.45
5	0.29	0.20	1.0	0.40	0.60
6	0.29	0.20	1.5	0.30	0.70

Table 2
Compact nozzle response of a subsonic nozzle due to an acoustic forcing at the inlet.

wave	α^{i-}			α^{e+}		
transfer function	$\dfrac{\bar{M}^e - \bar{M}^i}{1 - \bar{M}^i}$	$\dfrac{1 + \bar{M}^i}{\bar{M}^i + \bar{M}^e}$	$\dfrac{1 - \frac{1}{2}(\gamma - 1)\bar{M}^e\bar{M}^i}{1 + \frac{1}{2}(\gamma - 1)\bar{M}^e\bar{M}^i}$	$\dfrac{2\bar{M}^e}{1 + \bar{M}^e}$	$\dfrac{1 + \bar{M}^i}{\bar{M}^i + \bar{M}^e}$	$\dfrac{1 + \frac{1}{2}(\gamma - 1)\bar{M}^e\bar{M}^e}{1 + \frac{1}{2}(\gamma - 1)\bar{M}^e\bar{M}^i}$

the combustor that is important in the study of thermoacoustic instabilities, as they can perturb the rate of combustion heat release [52, 53]. Two key aspects of the phase plots are noted. First, the presence of a phase shift in the waves generated by the bypass stream in Fig. 9 and the absence thereof in Fig. 10, in which the initial mean flow Mach number of the bypass was held constant, indicates that the phase of the waves is predominantly governed by the inflow Mach number. Second, the curves produced by the jet and bypass streams are offset by a time delay that is dependent on frequency. The delay is not observed in the compact solution at the limit of zero frequency, but it increases linearly with frequency thereafter. The linear phase behavior is expected as the spatial length of the nozzle acts as a phase shifter. The magnitude of the offset between the curves can be linked to the mean flow Mach number of each stream at the inlet. The waves will be perfectly in-phase when the difference in inflow Mach numbers is zero, i.e., $\Delta = \left|\bar{M}^i_{\text{jet}} - \bar{M}^i_{\text{bypass}}\right| = 0$.

4.2. Response due to an acoustic excitation

Figs. 11 and 12 show the acoustic response due to an acoustic forcing at the inlet for the same conditions described in Section 4.1. This forcing can be thought of as a local density variation in the mean flow, that propagates at the speed of sound and arises due to the unsteady heat release in the combustor upstream of the nozzle. It can be seen that the lowest bypass inflow Mach number results in the largest acoustic transfer function at the exit. Physically, this means that direct noise is greater in the bypass stream and it is most amplified at low inflow and outflow Mach numbers. Leyko, Nicoud & Poinsot [11] arrived to the same conclusion when they calculated indirect-to-direct noise ratios below unity at low Mach numbers. Looking at Fig. 12b, we observe that the transmitted transfer functions of each stream fall into a single curve. This indicates that they are independent of the mean flow Mach number profile. A similar observation was reported by Duran & Moreau [23] in their study of single stream subsonic nozzles. Interestingly, the magnitude of the reflected transfer functions of the bypass stream remains higher than the jet at all frequencies considered and increases as the inflow Mach number increases and bypass ratio decreases. To explain this, we refer to the compact nozzle solution derived by Marble & Candel [18] for a single stream nozzle (Table 2). From the expressions, it can be deduced that the reflected acoustic wave is proportional to $(\bar{M}^e - \bar{M}^i)/(\bar{M}^i + \bar{M}^e)$, while the transmitted acoustic wave is inversely proportional to $(\bar{M}^i + \bar{M}^e)$. Since the high-speed, core jet stream experiences weaker accelerations and decelerations in the compound nozzle, the difference, $\bar{M}^e_{\text{jet}} - \bar{M}^i_{\text{jet}}$, is relatively small when compared to that of the bypass stream. Furthermore, due to the higher inflow Mach number of the jet, the sum of Mach numbers, $\bar{M}^e_{\text{jet}} + \bar{M}^i_{\text{jet}}$, is large. Thus, smaller transfer functions are obtained from the jet. As for the bypass stream, we note that stronger mean flow gradients cause the difference, $\bar{M}^e_{\text{bypass}} - \bar{M}^i_{\text{bypass}}$, to grow much more rapidly than the sum, $\bar{M}^e_{\text{bypass}} + \bar{M}^i_{\text{bypass}}$. Hence, the highest bypass Mach number at the inlet, $\bar{M}^i_{\text{bypass}} = 0.15$, and lowest bypass ratio, BPR = 0.5, yield the largest reflected transfer functions. Finally, we also note that a minimal phase shift is present in the phase plots. As the incoming acoustic forcing at the inlet propagates at the speed of sound

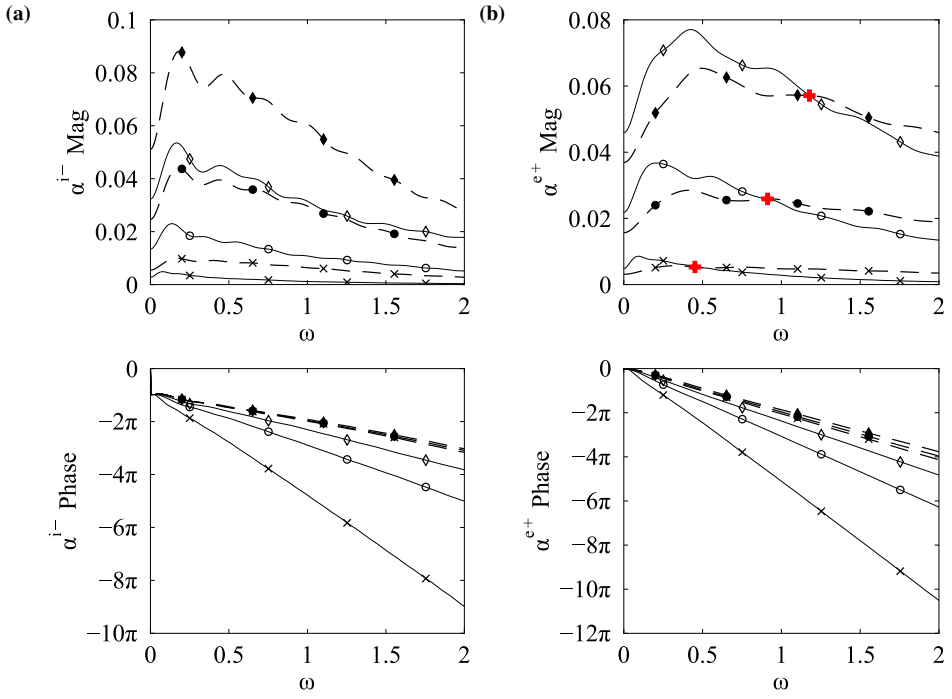

Fig. 9. Magnitude and phase of (a) α^{i-} and (b) α^{e+} caused by $\beta^i = 1.0$ for $\bar{M}^i_{\text{bypass}} = [0.05\text{–}0.15]$. Recall that (×): $\bar{M}^i_{\text{bypass}} = 0.05$, (○, ●): $\bar{M}^i_{\text{bypass}} = 0.1$, and (◇, ◆): $\bar{M}^i_{\text{bypass}} = 0.15$. Dashed lines (— —) refer to the jet stream; solid lines (——) refer to the bypass; and red crosses (+) indicate the threshold frequency ω_{th}.

and the inflow and outflow Mach numbers in all cases remain well in the subsonic regime, the time lag between the resulting waves is not significant.

4.3. Effect of mass-averaging properties

It is interesting to compare the indirect noise generated from a multi-stream compound nozzle with an equivalent single stream nozzle. In this subsection, the acoustic response due to an entropic excitation of a compound nozzle is compared with a single stream nozzle with mass-averaged properties. Here, we select $\bar{M}^i_{\text{jet}} = 0.29$, $\bar{M}^i_{\text{bypass}} = 0.05$, and BPR = 1.0 (Case 1 from Table 1) for the compound case. An equivalent, mass-averaged, single stream nozzle has $\bar{M}^i_{\text{jet}} = \bar{M}^i_{\text{bypass}} = 0.085$ at the inlet. All other conditions including the nozzle geometry remain the same as those described earlier in this section. The mean flow Mach number distribution of both cases is plotted in Fig. 13a. To ensure a grid independent solution, a grid refinement study is conducted and the acoustic response at the inlet obtained from different nozzle subdivisions is plotted in Fig. 13b for the single stream, mass-averaged case. As can be seen, 20,000 nozzle subdivisions is sufficient for grid independence. The acoustic response from both nozzles is computed in Fig. 14. We note that the responses are distinct, despite the mass-averaging of properties. Namely, indirect noise generation in the multi-stream nozzle is smaller than the mass-averaged, single stream nozzle in the low-mid frequency range ($\omega < 1.55$). This is expected as the streams in the compound nozzle undergo gradual spatial accelerations and decelerations. Whereas, the single stream in the mass-averaged nozzle undergoes more abrupt changes in mean flow properties. At high frequencies, the jet stream of the compound nozzle produces more indirect noise. This is due to the fact that, in the absence of strong mean flow gradients, the frequency response of the jet deviates very little from and can be approximated by the compact solution at zero frequency. Similarly, the responses obtained from the bypass and the mass-averaged, single stream decay exponentially with increasing frequency due to the presence of spatial mean flow gradients. From Fig. 14a, it can be seen that the reflected acoustic wave produced by the jet is larger than that produced by the mass-averaged, single stream over most frequencies. These stronger reflections can be attributed to the higher jet throat Mach number. Lastly, the trends observed in the phase plots confirm the findings in Section 4.1,

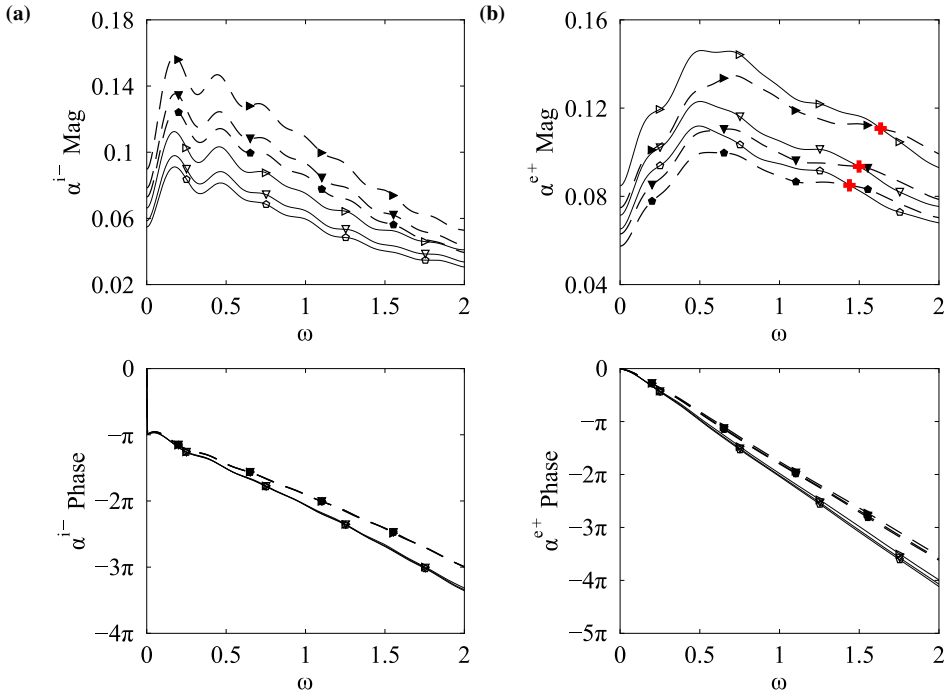

Fig. 10. Magnitude and phase of (a) α^{i-} and (b) α^{e+} caused by $\beta^i = 1.0$ for BPR = [0.5–1.5]. Recall that (▷, ▶): BPR = 0.5, (▽, ▼): BPR = 1.0, and (⬠, ⬟): BPR = 1.5; (— —) jet stream; (——) bypass stream; and (+) ω_{th}.

in which it was found that the inflow Mach number governs the time delay between the resulting waves and the nozzle length acts as a linear phase shifter. Nonetheless, the striking differences present in the acoustic responses further highlight the need for a robust analytical tool capable of computing the acoustic and entropic transfer functions of arbitrary multi-stream, compound nozzle flows.

5. Conclusions

Compound-compressible nozzles, where multiple gas streams are exhausted side by side, have applications in supersonic ejector-mixer nozzles and in engine test facilities. A low-order analytical model was developed to compute the transfer functions and quantify the indirect noise generated from each stream in a compound-compressible nozzle setting. The model extends the previous work of Duran & Moreau [23] by using the fundamental equations governing compound flow derived by Bernstein, Heiser & Hevenor [36]. The main assumptions taken in the model are negligible mixing between the inviscid streams, constant radial pressure, and the shear layer acts as a waveguide to the perturbations. The model was validated against analytical results and numerical simulations.

A parametric study was conducted on a dual stream nozzle, spanning a range of bypass Mach numbers and bypass ratios at the inlet. For each case, the acoustic response was obtained for unitary entropic and acoustic excitations at the inlet. It was shown that the acoustic signature of each stream varies significantly depending on the bypass inflow conditions. In general, increasing the inflow Mach number or decreasing the bypass ratio yields stronger accelerations and decelerations of the flow in the nozzle. This, in turn, translates to more amplified responses from entropic perturbations. We also note that the phase of the resulting waves is greatly affected by the initial bypass Mach number. For acoustic excitations at the inlet, the largest reflected transfer functions were obtained from the highest bypass inflow Mach number and lowest bypass ratio. Additionally, the transmitted transfer functions were shown to be independent on the evolution of the mean flow Mach number through the nozzle. An important outcome of the analysis is that indirect noise generation in the lower speed, peripheral bypass flow can exceed that of the higher speed, core jet flow at certain frequencies. The acoustic response of the compound nozzle was also compared with an

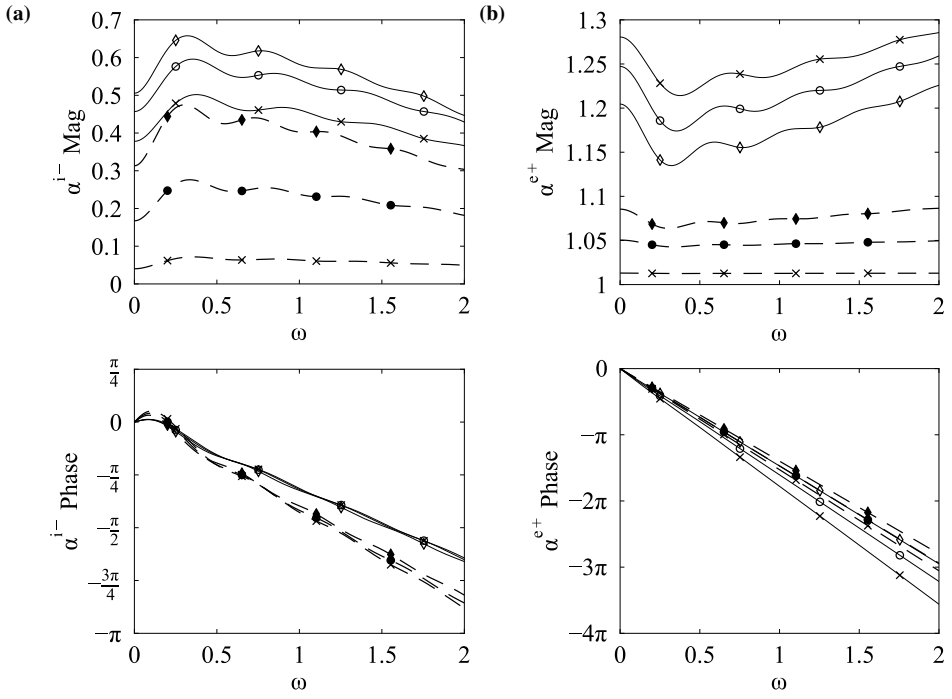

Fig. 11. Magnitude and phase of (a) α^{i-} and (b) α^{e+} caused by $\alpha^{i+} = 1.0$ for $\bar{M}^{i}_{\text{bypass}} = [0.05\text{–}0.15]$. Recall that (×): $\bar{M}^{i}_{\text{bypass}} = 0.05$, (○, ●): $\bar{M}^{i}_{\text{bypass}} = 0.1$, and (◇, ♦): $\bar{M}^{i}_{\text{bypass}} = 0.15$. Dashed lines (— —) refer to the jet stream; and solid lines (——) refer to the bypass.

equivalent single stream nozzle with mass-averaged properties. It was shown that the responses from both nozzles are distinct, further establishing the need for developing a tool to analyze multi-stream nozzle flows.

The proposed mathematical model could be used to provide preliminary design and noise assessments of future aeroengines, engine test facilities, and ejector-mixer nozzles. The model can be improved by relaxing the constant radial pressure assumption by considering two-dimensional effects and by accounting for mixing between the streams before solving the compound flow equations. Both of these assumptions will be subject to future investigations.

Acknowledgments

We acknowledge the support of the Natural Sciences and Engineering Research Council of Canada (NSERC), the Ontario Centres of Excellence (OCE), and MDS Aero Support Corporation. Fruitful discussions with Dr. Ignacio Duran, Dr. Gley Zitouni, Mr. Jag Rajasekaran, and Dr. David Arthurs are acknowledged. Computations were performed on the Niagara supercomputer at the SciNet HPC Consortium. SciNet is funded by: the Canada Foundation for Innovation under the auspices of Compute Canada; the Government of Ontario; Ontario Research Fund - Research Excellence; and the University of Toronto.

Appendix A. Wavenumber Analysis

To assess the validity of OpenFOAM v17.12 in resolving the planar acoustic waves and to quantify the dispersive and dissipative errors of the numerical schemes implemented, the propagation of a periodic signal in a stationary base flow is studied. The input disturbance is given by a sinusoidal function as follows:

$$q(t) = \bar{p} + A sin(\omega t), \tag{A.1}$$

where the mean flow pressure, $\bar{p} = 101.325$ kPa, amplitude, $A = 0.1$ kPa, and angular frequency, $\omega = 2\pi f$ with $f = 1$ kHz. The wavenumber, k, is related to the wavelength λ by: $k = \frac{2\pi}{\lambda}$. The wavenumber can be related to the

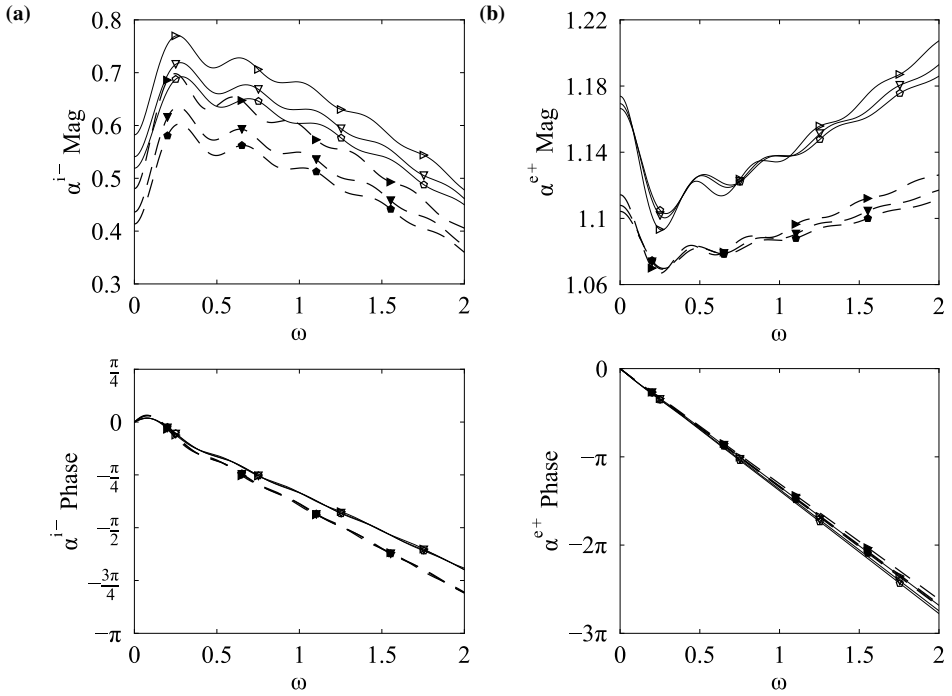

Fig. 12. Magnitude and phase (a) α^{i-} and (b) α^{e+} caused by $\alpha^{i+} = 1.0$ for BPR = [0.5–1.5]. Recall that (▷, ▶): BPR = 0.5, (▽, ▼): BPR = 1.0, and (⬠, ⬟): BPR = 1.5; (— —) jet stream; and (——) bypass stream.

temporal frequency of a sine wave using $\omega t = kx$, where x is the spatial dimension. The numerical setup consists of a straight one-dimensional duct of length, $L = 35\lambda$; the large domain is chosen as to avoid spurious boundary influence on the solution. The propagation of the disturbance is computed at a downstream location: $x_1 = 4\lambda$, for different grid resolutions; x_1 corresponds to a much longer propagation distance compared to the present results in Section 4. Here, we define the number of grid points per wavelength (*ppw*) as a measure of the grid resolution. In terms of the wavenumber, ppw can be written as:

$$\text{ppw} = \frac{2\pi}{k\Delta x}. \tag{A.2}$$

The non-dimensional pressure, $p' = (p - \bar{p})/A$, is plotted against dimensionless time, $\tau = tf$, in Fig. A.1 at x_1. Since the response is symmetric and periodic, only one cycle is visualized. The magnitude of the accumulated numerical error defined as $|p'_{numerical} - p'_{analytical}|$ is also shown. From these results, we can conclude that the numerical solver is validated and a minimum ppw = 100 is needed to achieve an error of $\leq 2\%$. We note that the solver shows poor properties for general aeroacoustic simulations, but given the high resolution and short propagation distance used in our simulations, it is deemed acceptable.

References

[1] A. P. Dowling and Y. Mahmoudi, "Combustion noise," *Proceedings of the Combustion Institute*, vol. 35, no. 1, pp. 65–100, 2015.

[2] M. Ihme, "Combustion and Engine-Core Noise," *Annual Review of Fluid Mechanics*, vol. 49, pp. 227–310, 2017.

[3] W. C. Strahle, "Some results in combustion generated noise," *Journal of Sound and Vibration*, vol. 23, no. 1, pp. 113–125, 1972.

[4] H. A. Hassan, "Scaling of combustion generated noise," *Journal of Fluid Mechanics*, vol. 66, no. 3, pp. 445–453, 1974.

[5] R. Rajaram and T. Lieuwen, "Acoustic radiation from turbulent premixed flames," *Journal of Fluid Mechanics*, vol. 637, pp. 357–385, 2009.

[6] N. Swaminathan, G. Xu, A. P. Dowling, and P. Balachandran, "Heat release rate correlation and combustion noise in premixed flames," *Journal of Sound and Vibration*, vol. 681, pp. 80–115, 2011.

[7] M. Talei, M. J. Brear, and E. R. Hawkes, "Sound generation by laminar premixed flame annihilation," *Journal of Fluid Mechanics*, vol. 679, pp. 194–218, 2011.

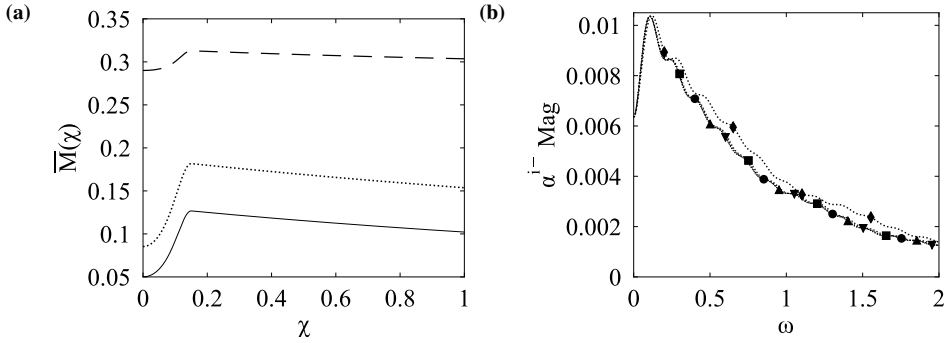

Fig. 13. (a) Mean flow Mach number distribution through the compound nozzle and the single stream, mass-averaged nozzle and (b) results from the grid refinement study conducted on the single stream case, where $\bar{M}^i_{\text{jet}} = \bar{M}^i_{\text{bypass}} = 0.085$ and BPR = 1.0. (— —): jet stream; (——): bypass stream; and (· · · · ·): mass-averaged stream. (⧫): 1000; (■): 5000; (●): 10,000; (▲): 20,000; and (▼): 30,000 subdivisions.

[8] M. Ihme and H. Pitsch, "On the generation of direct combustion noise in turbulent non-premixed flames," *International Journal of Aeroacoustics*, vol. 11, no. 1, pp. 25–78, 2012.

[9] S. Candel, *Analytical Studies of Some Acoustic Problems of Jet Engines*. PhD thesis, 1972.

[10] M. Leyko, F. Nicoud, S. Moreau, and T. Poinsot, "Numerical and analytical investigation of the indirect combustion noise in a nozzle," *Comptes Rendus Mécanique*, vol. 337, no. 6-7, pp. 415–425, 2008.

[11] M. Leyko, F. Nicoud, and T. Poinsot, "Comparison of Direct and Indirect Combustion Noise Mechanisms in a Model Combustor," *AIAA Journal*, vol. 47, no. 11, pp. 2709–2716, 2009.

[12] M. S. Howe, "Indirect combustion noise," *Journal of Fluid Mechanics*, vol. 659, pp. 267–288, 2010.

[13] L. Rayleigh, *The Theory of Sound*. London: Macmillan and co., 1877.

[14] L. Crocco, "Research on combustion instability in liquid propellant rockets," in *Proceedings of the 12th International Symposium on Combustion*, pp. 85–99, The Combustion Institute, 1969.

[15] G. Wang, M. Sanjose, S. Moreau, D. Papadogiannis, F. Duchaine, and L. Gicquel, "Noise mechanisms in a transonic high-pressure turbine stage," *International Journal of Aeroacoustics*, vol. 15, no. 1-2, pp. 144–161, 2016.

[16] A. Holewa, S. Lesnik, G. Ashcroft, and S. Guérin, "CFD-Based Investigation of Turbine Tonal Noise Induced by Steady Hot Streaks," *International Journal of Turbomachinery, Propulsion and Power*, vol. 2, no. 1, pp. 3–18, 2017.

[17] H. S. Tsien, "The Transfer Functions of Rocket Nozzles," *Journal of the American Rocket Society*, vol. 22, no. 3, pp. 139–143, 1952.

[18] F. E. Marble and S. M. Candel, "Acoustic disturbance from gas non-uniformities convected through a nozzle," *Journal of Sound and Vibration*, vol. 55, no. 2, pp. 225–243, 1977.

[19] W. H. Moase, M. J. Brear, and C. Manzie, "The forced response of choked nozzles and supersonic diffusers," *Journal of Fluid Mechanics*, vol. 585, pp. 281–304, 2007.

[20] A. Giauque, M. Huet, and F. Clero, "Analytical Analysis of Indirect Combustion Noise in Subcritical Nozzles," *Journal of Engineering for Gas Turbines and Power*, vol. 134, no. 11, pp. 111–202, 2012.

[21] S. R. Stow, A. P. Dowling, and T. P. Hynes, "Reflection of circumferential modes in a choked nozzle," *Journal of Fluid Mechanics*, vol. 467, pp. 215–239, 2002.

[22] C. S. Goh and A. S. Morgans, "Phase prediction of the response of choked nozzles to entropy and acoustic disturbances," *Journal of Sound and Vibration*, vol. 330, no. 21, pp. 5184–5198, 2011.

[23] I. Duran and S. Moreau, "Solution of the quasi-one-dimensional linearized Euler equations using flow invariants and the Magnus expansion," *Journal of Fluid Mechanics*, vol. 723, pp. 190–231, 2013.

[24] W. Magnus, "On the exponential solution of differential equations for a linear operator," *Communications on Pure and Applied Mathematics*, vol. 7, no. 4, pp. 649–673, 1954.

[25] S. Blanes, F. Casas, J. A. Oteo, and J. Ros, "The Magnus expansion and some of its applications," *Physics Reports*, vol. 470, pp. 151–238, 2009.

[26] I. Duran and A. S. Morgans, "On the reflection and transmission of circumferential waves through nozzles," *Journal of Fluid Mechanics*, vol. 773, pp. 137–153, 2015.

[27] L. Magri, J. O'Brien, and M. Ihme, "Compositional inhomogeneities as a source of indirect combustion noise," *Journal of Fluid Mechanics*, vol. 799, no. R4, pp. 1–12, 2016.

[28] L. Magri, "On indirect noise in multicomponent nozzle flows," *Journal of Fluid Mechanics*, vol. 828, no. R2, pp. 1–13, 2017.

[29] C. Kodres and G. Murphy, "Jet-engine test cell augmenter performance," *Journal of Propulsion and Power*, vol. 14, no. 2, pp. 129–134, 1998.

[30] L. T. Clark, "Application of compound flow analysis to supersonic ejector-mixer performance prediction," in *33rd Aerospace Sciences Meeting and Exhibit, Aerospace Sciences Meetings*, (Reno), AIAA, 1995.

[31] T. G. Tillman, R. W. Paterson, and W. M. Presz Jr., "Supersonic Nozzle Mixer Ejector," *Journal of Propulsion and Power*, vol. 8, no. 2, pp. 513–519, 1992.

[32] M. Yonamine, T. Ushijima, Y. Miyazato, M. Masuda, H. Katanoda, and K. Matsuo, "Propagation of weak pressure waves against two parallel subsonic streams," *Journal of Thermal Science*, vol. 15, no. 2, pp. 135–139, 2006.

[33] M. Férand, G. Daviller, S. Moreau, C. Sensiau, and T. Poinsot, "Using LES for combustion noise propagation to the far-field by considering

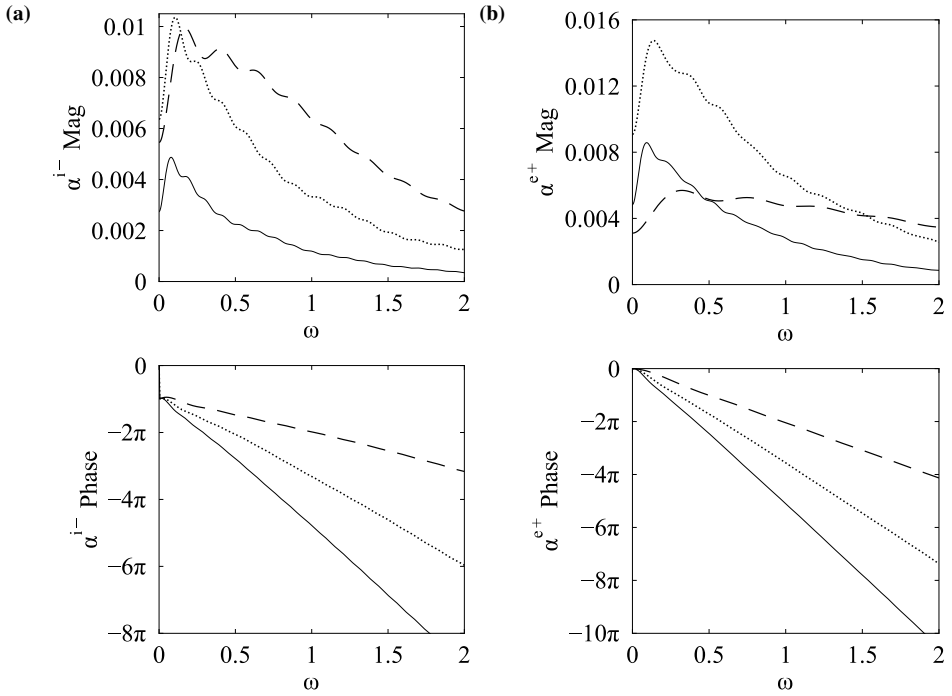

Fig. 14. Magnitude and phase of (a) α^{i-} and (b) α^{e+} caused by $\beta^i = 1.0$. Dashed lines (— —) refer to the jet stream; solid lines (——) refer to the bypass; and dotted lines (· · · · ·) refer to the mass-averaged stream.

the jet flow of a dual-stream nozzle," in *AIAA/CEAS Aeroacoustics Conference*, (Atlanta, Georgia), 2018.

[34] H. Pearson, J. B. Holliday, and S. F. Smith, "Theory of the cylindrical ejector supersonic propelling nozzle," *Journal of the Royal Aeronautical Society*, vol. 62, no. 574, pp. 746–751, 1958.

[35] H. J. Hoge and R. A. Segars, "Choked flow - A generalization of the concept and some experimental data," *AIAA Journal*, vol. 3, no. 12, pp. 2177–2183, 1965.

[36] A. Bernstein, W. H. Heiser, and C. Hevenor, "Compound-Compressible Nozzle Flow," *ASME Journal of Applied Mechanics*, vol. 34, no. 3, pp. 548–554, 1967.

[37] A. H. Shapiro, *The dynamics and thermodynamics of compressible fluid flow*. New York: Ronald Press Co., 1953.

[38] A. M. Agnone, "Comment on 'Choked Flow: A Generalization of the Concept and Some Experimental Data'," *AIAA Journal*, vol. 9, no. 4, pp. 0768a–0768a, 1971.

[39] D. R. Otis, "Choking and Mixing of Two Compressible Fluid Streams," *Journal of Fluids Engineering*, vol. 98, no. 2, pp. 311–317, 1976.

[40] J.-K. Kwon, K. Masusaka, Y. Miyazato, M. Masuda, K. Matsuo, and H. Katanoda, "Compound Choking of a Two-Parallel Stream Through a Convergent Duct," *KSME International Journal*, vol. 15, no. 12, pp. 1829–1834, 2001.

[41] E. M. Greitzer, C. S. Tan, and M. B. Graf, *Internal Flow: Concepts and Applications*. Cambridge: Cambridge University Press, 2004.

[42] N. H. Saiyed, K. L. Mikkelsen, and J. E. Bridges, "Acoustics and Thrust of Separate-Flow Exhaust Nozzles With Mixing Devices for High-Bypass-Ratio Engines," tech. rep., 2000.

[43] J.-N. Hau and B. Müller, "Acoustic wave propagation in a temporal evolving shear-layer for low-Mach number perturbations," *Physics of Fluids*, vol. 30, no. 016105, pp. 1–14, 2018.

[44] J.-P. Hickey, F. Hussain, and X. Wu, "Compressibility effects on the structural evolution of transitional high-speed planar wakes," *Journal of Fluid Mechanics*, vol. 796, pp. 5–39, 2016.

[45] W. A. Bell, B. R. Daniel, and B. T. Zinn, "Experimental and theoretical determination of the admittances of a family of nozzles subjected to axial instabilities," *Journal of Sound and Vibration*, vol. 30, no. 2, pp. 179–190, 1973.

[46] H. G. Weller, G. Tabor, H. Jasak, and C. Fureby, "A tensorial approach to computational continuum mechanics using object-oriented techniques," *Computers in Physics*, vol. 12, no. 6, pp. 620–631, 1998.

[47] J. D. Anderson, *Modern Compressible Flow: With Historical Perspective*. New York: McGraw-Hill, second ed., 1990.

[48] The OpenFOAM Foundation, "OpenFOAM Extended Code Guide," 2017.

[49] T. J. Poinsot and S. K. Lelef, "Boundary conditions for direct simulations of compressible viscous flows," *Journal of Computational Physics*, vol. 101, pp. 104–129, 1992.

[50] C. Van Loan, *Computational Frameworks for the Fast Fourier Transform*. Ithaca, New York: Society for Industrial and Applied Mathematics, 1992.

[51] C. S. Goh and A. S. Morgans, "The influence of entropy waves on the thermoacoustic stability of a model combustor," *Combustion Science and Technology*, vol. 185, no. 2, pp. 249–268, 2013.

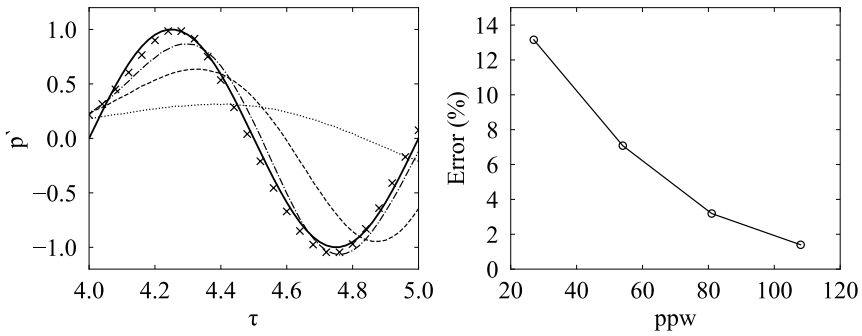

Fig. A.1. Non-dimensional pressure, p', and accumulated error at $x_1 = 4\lambda$ using a sinusoidal input. (——): analytical; (· · · · ·): 27; (— —): 54; (— ·): 81; and (×): 108 grid points per wavelength.

[52] A. Dowling, "The calculation of thermoacoustic oscillations," *Journal of Sound and Vibration*, vol. 180, no. 4, pp. 557–581, 1995.

[53] D. Papadogiannis, G. Wang, S. Moreau, F. Duchaine, L. Gicquel, and F. Nicoud, "Assessment of the Indirect Combustion Noise Generated in a Transonic High-Pressure Turbine Stage," *Journal of Engineering for Gas Turbines and Power*, vol. 138, no. 4, p. 041503, 2015.